International Journal of Mechanical Sciences 61 (2012) 32–43

Contents lists available at SciVerse ScienceDirect

International Journal of Mechanical Sciences

journal homepage: www.elsevier.com/locate/ijmecsci

Contact impingement in packings of elastic–plastic spheres, application to powder compaction

Barthélémy Harthong [a], Jean-François Jérier [a], Vincent Richefeu [a], Bruno Chareyre [a], Pierre Dorémus [a], Didier Imbault [a], Frédéric-Victor Donzé [a,b,*]

[a] Grenoble-INP, Université Joseph Fourier, UMR 5521, Laboratoire Sols, Solides, Structures - Risques, UMR 5521, Domaine Universitaire, BP 53, 38041 Grenoble Cedex 9, France
[b] CSIRO, Earth Science and Resource Engineering, Queensland Centre for Advanced Technologies, 1 Technology Court, Pullenvale 4069, Australia

ARTICLE INFO

Article history:
Received 15 February 2011
Received in revised form
26 April 2012
Accepted 30 April 2012
Available online 7 May 2012

Keywords:
Granular materials
Powder compaction
High density
Contact model
Discrete-element method
Finite-element method

ABSTRACT

High-density compaction of ductile powder particles is characterized by a sharp increase of the inter-particle normal contact force. This is due to both complex contact interactions and plastic incompressibility of the particle constitutive material. A DEM model (OPEN-DEM YADE) using an interaction force-law reproducing this increase has been developed to simulate high-density compaction of ductile powders. Its formulation is derived from a Finite Element Method model (ABAQUS). Macroscopic stresses resulting from compaction tests carried out on a random assembly of spherical grains were computed with both models and then compared. A good agreement between the stress–density curves confirmed the accuracy of the DEM formulation. However, the role of the grain deformation may not be well described using DEM since it is based on an assumption of overlapping rigid particles but allows low calculation costs. To highlight the role of this deformation process, a detailed FEM-based analysis of the influence of contact impingement on the normal contact force is thus presented. It explores the mechanisms of stress transmission between contact zones and quantifies the appearance of contact interactions in terms of both indentation depth and relative density. Results show that contact impingement cannot be neglected at a relative density as low as 0.7 if a local, contact-scale analysis is aimed for (such as density distribution for instance). In such a case, previous models like the one proposed by Storåkers and co-authors, should be used with care. The local solid fraction provides a correct local description of both contact interactions and plastic incompressibility of the constitutive material of the grains up to the maximum density. This would allow the DEM to be successfully applied to large-scale simulations of high-density compaction.

1. Introduction

Powder metallurgy has long been an attractive technology for both advanced and conventional materials. The material properties can be obtained by mixing different powder materials and producing near net shape parts which is the major advantage of this method. In many applications, powder parts are compacted up to a relative density as high as possible (more than 0.95), for strength and homogeneity. A numerical tool which would properly predict the mechanical constitutive behavior of the powder during all the forming process is a key issue for manufacturers. With this in mind, plasticity and elasticity phenomena, internal friction of the porous medium and frictional effects between the die walls must be considered. Continuum models based on Drucker Prager Cap model [12,11] are currently used by industrials, but they are limited for several basic applications, such as the calculation of stresses during compaction [14]. Such models are based on complex and expensive experimental devices, which only give information on few loading paths. As a result, they fail to describe the material's behavior for other loadings or complex loading histories. To overcome this problem, and to further understand the complex relations between the grains behavior and the aggregates behavior, the problem of the mechanical behavior of powders has been addressed from a micromechanical perspective. Arzt [3], for instance, studied the influence of the coordination number on the compaction and sintering of powders. A micromechanical model is then proposed by Fischmeister and Artz [15] by assuming that the movement of the particles can be described as an isotropic homogeneous densification. Fleck et al. [17], then Fleck [16] and Storåkers et al. [44] proposed a model for the first part of compaction (stage I compaction), by applying a homogeneous strain field to the particles. This model has been compared with experiments by Akisanya et al. [2],

* Corresponding author at: CSIRO, Earth Science and Resource Engineering, Queensland Centre for Advanced Technologies, 1 Technology Court, Pullenvale 4069, Australia.
E-mail address: frederic.donze@hmg.inpg.fr (F.-V. Donzé).

0020-7403/$ - see front matter Crown Copyright © 2012 Published by Elsevier Ltd. All rights reserved.
http://dx.doi.org/10.1016/j.ijmecsci.2012.04.013

Sridhar and Fleck [42] and Cocks [8]. Cocks and Sinka [9] and Sinka and Cocks [40] carried out investigations on similar bases, while presenting a framework for the modeling and the experimental calibration of powder compaction.

Over the last decade, the Discrete Element Method (DEM) [10] has been applied to the compaction of powders. Heyliger and McMeeking [24] and Martin [32] compared results from the DEM to a homogeneous strain field model. Several studies have been carried out, such as those of Martin and Bouvard [33], Martin et al. [34], Skrinjar and Larsson [41], Pizette et al. [36]. The core of the DEM is the contact law, which describes the relationship between the contact force and the relative displacement of two particles in contact. For cold compaction of metal powders, it is commonly assumed that the main phenomenon to be studied at the contact scale is plasticity. Therefore, the right contact laws to be used have to describe correctly the plastic indentation of two solid particles. Vu-Quoc and Zhang [46] and Vu-Quoc et al. [47] proposed a contact model accounting for plasticity, but their model is valid in the context of granular flows, where the deformations involved remain very small. However, the problem of plastic indentation of two particles is to be put together with the Brinell or Vickers indentation problem [28,25]. In this context, Storåkers et al. [43] have developed a plastic contact law for power-law strain-hardening solids, which has been intensively applied in DEM simulations and homogeneous strain field modeling of powder compaction by most of the previously cited authors. But the modeling of powder compaction by the discrete element method up to a relative density higher than 0.8–0.85 is not yet valid, because the implementation of such contact laws in micromechanical models has the major inconvenient of considering the mechanical and geometrical independence of contacts during the densification. Preliminary studies by Harthong et al. [23] introduced a high-density contact law for the DEM based on finite element simulations.

In parallel, another discrete numerical approach based on the finite-element method has emerged. Here, this method will be referred to as the Multi-Particle Finite Element Method (MPFEM) [21,20,48,38]. It has the significant advantage of describing very accurately the deformation and the movement of the particles, and to be usable with classical and well-known constitutive laws to describe the particle material. The main limitation of the method is the calculation time needed when considering assemblies of numerous meshed particles. First developed for two-dimensional particles, it has been applied recently to 3D particles by Chen [6,7] and Frenning [18,19]. Using this method, Schmidt et al. [39] and Harthong et al. [22] derived yield surfaces from an assembly of 3D elastic–plastic meshed particles.

Both DEM and MPFEM may be powerful tools to understand the microstructural phenomena which lead to the well-known or less-known macroscopic aspects of powder compaction. Both methods consist in representing the powder by discrete particles (assumed spherical in most cases) and modeling the interaction between the particles. However, the computational cost of the MPFEM remains too high to perform simulations on a realistic number of particles, even though it gives more information and it appears more accurate and reliable. This is the reason why the DEM appears as the best practical compromise between accuracy and calculation efficiency.

The new contact law for the DEM presented in Harthong et al. [23] was validated on the basis of DEM and MPFEM frictionless simulations on a 32-sphere assembly. The aim of the present paper is to present an analysis of the mechanisms of complex interactions at contact zones between grains in the context of high-density compaction. This analysis is focused on a DEM application, and thus underlines and explains the limits of a previous model [43] in an application such as powder metallurgy, which have never been discussed before. This is the reason why, after a short description of the main features of DEM and MPFEM in Section 2, the first part of this paper details, in Section 3, the DEM implementation of a contact model based on Harthong et al. [23]. These DEM simulations are used as a basis to understand the relations between contact models and overall or macroscopic behavior. Section 4 finally discusses the results of the contact models using MPFEM results as a reference.

2. MPFEM and DEM approaches

2.1. Multi-particle finite element method

The multi-particle finite element method (MPFEM) consists in performing classical finite element simulations on an assembly of discrete particles. These particles are meshed and their interactions are ruled by classical finite-element contact conditions. In the present work, the method has been applied by using the finite element code ABAQUS. The interactions are modeled by a penalty contact algorithm, where the nodal forces are proportional to the penetration between the surfaces, and by a Coulomb friction with a friction coefficient f (with the same value for both sphere/sphere and sphere/wall contacts). The details of the contact modeling and finite element implementation can be found in ABAQUS [1]. No contact cohesion was considered here.

The constitutive law of individual particles corresponds to a Von-Mises type, elastic–plastic material with strain hardening. The evolution of the yield surface is calculated through a power-law:

$$\sigma = \sigma_0 \varepsilon^{1/m} \tag{1}$$

where σ and ε are respectively the Von Mises equivalent stress and strain, σ_0 is the hardening modulus, and $1/m$ is the plastic exponent. The elastic part is assumed linear and isotropic, with elastic modulus E and Poisson's coefficient v.

Previous studies by Chen et al. [6,7], comparing experimental and numerical results, involved lead alloy as the constitutive material of the particles. We chose the same material, with the following numerical values of E, v, σ_0 and m:

$$\begin{cases} E = 10,000 \text{ MPa} \\ v = 0.435 \\ \sigma_0 = 20.5 \text{ MPa} \\ m = 4.16 \end{cases} \tag{2}$$

The same authors [6,7] also determined the value of the friction coefficient between lead spheres to be $f=0.1$ on the basis of numerical simulation and literature search ([4] for instance). Moreover, the choice of such a low value was very convenient to reduce the calculation time required for the MPFEM simulations.

The mesh was designed to provide a correct description of the contact forces at the local scale. It includes 2600 quadratic tetrahedral elements per sphere (Fig. 2).

2.2. Discrete element method

In DEM, spherical particles are not meshed and can be defined only with the coordinates of their center, their radius and mass. For each increment of time, the center-to-center distances are calculated. Usually, deformation is supposed to occur only in a small contact zone so that the relative displacement h_{ij} between particles i and j is enough to represent the deformation, and to evaluate a force F_{ij} from a so-called *force-law*; see Fig. 1. In other words, particles are rigid but contact deformation is modeled anyway, with the help of the overlap h_{ij}. At a given time step, the total force and moment acting on the mass center of each particle

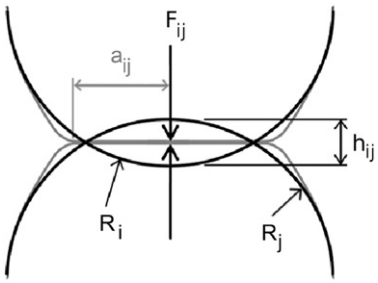

Fig. 1. Indentation of two spheres.

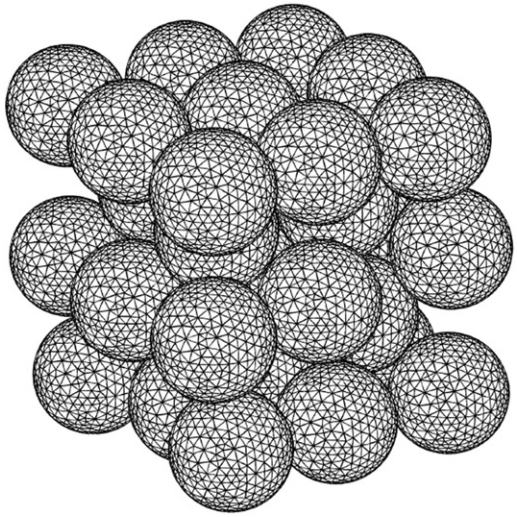

Fig. 2. 32-Sphere random packing (here in the case of MPFEM).

are used to compute its acceleration. The positions of the particles are then obtained from the integration of Newton's equations.

The high-density model and the similarity solution from Storåkers et al. [43] were implemented in the open-source code YADE [29,30,45] to study the response of random assemblies of spheres. To this end, the force-law was completed by a simplified elastic and friction force-law. As for MPFEM simulations, no cohesion was considered here. At high-density, the deformation of the particles can no longer be considered as localized, and the contact zones cannot be supposed independent. Since the relative displacement h_{ij} is a convenient variable, it is still used in the high-density model to compute the normal force. A second variable is added to account for the shape evolution of each particle and contact interactions. This variable is the local solid fraction which will be described in more details together with the contact models in Section 3.

2.3. 32-Sphere sample

For this study, we use a random assembly of 32 monosized spheres illustrated in Fig. 2. The initial assembly is strictly the same for both the MPFEM and DEM simulations. The only difference is that spheres are not meshed in the case of DEM simulations. This sample was generated using the discrete element approach by increasing the radius of each sphere in a fixed cube until the pressure stabilizes at a given value. The initial relative density is 0.48, and all particles have the same constitutive material. The loadings applied to this assembly are the classical isotropic and die compaction.

3. DEM simulations

As suggested before, classical DEM force-laws assume that contact zones are small and independent. When these assumptions are valid, h_{ij} is a convenient variable to describe contact deformation. Since the modeling of high-density compaction at least requires the description of interactions between neighboring contacts [34], the local solid fraction is added to formulate our high-density model.

In this section, the computation of the local solid fraction, which is needed for the high-density model, is first described in Section 3.1. With this parameter, an elastic–plastic high-density model can be defined using a plastic force obtained following Harthong et al. [23]. These modifications are introduced in Section 3.2. Comparison between MPFEM and DEM results are presented in Section 3.3.

3.1. Local solid fraction

To define a solid fraction at the particle scale, it is necessary to split the overall volume into smaller cells surrounding each particle such that the sum of all the cell volumes is equal to the overall volume. To achieve this, we use a radical Voronoi tessellation. The radical Voronoi graph is the dual of the weighted Delaunay triangulation (also called "regular" triangulation in [13]), where a weighted point $C^*=(C,w)$ can be seen as a sphere of center C and radius $R=\sqrt{w}$. Generally speaking, the Voronoi tessellation (radical or not) of a set of points C_i is a partition of the space assigning each point M of the space to the closest C_i. In the case of radical tessellation, the distance between a point M and a weighted point $C_i^*=(C_i,w_i)$ is defined as $\|MC_i^*\|^2=\|MC_i\|^2-w_i$ (this distance is MC_i in Fig. 3a). With this measure of distance, the set of points M equally distant from two weighted points C_i^* and C_j^* is a plane, called "radical" plane (Δ in Fig. 3a), and the portion of space associated to one sphere is a polyhedron (Figs. 3b and 4).

The radical tessellation of a set of weighted points $C_i^*=(C_i,w_i)$ is exactly the same as the usual Voronoi tessellation of the single points set C_i if all weights are equal, since bisector planes and radical planes coincide in that case. However, the "radical" variant has the advantage of giving a relevant partition even in the case of unequal diameters, in the sense that each particle will be inscribed in the corresponding cell-volume (see Fig. 3b). This feature was judged mandatory in anticipation of numerical simulations of non-uniform particle sizes, not presented here. The properties of radical tessellation also enabled the modeling of the rigid plates on each side of the packing as spheres of very large size (10^6 times the size of the packing), as seen in Fig. 3b. Based on this graph, the local solid fraction ρ_i assigned to a sphere

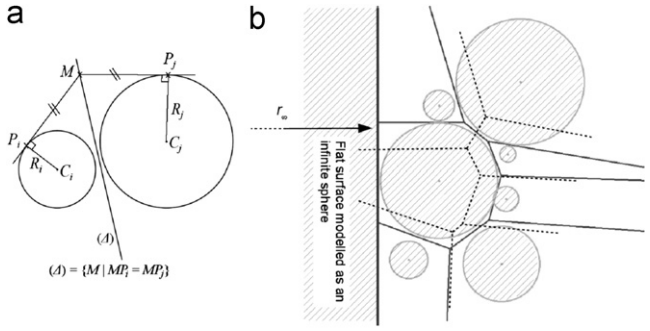

Fig. 3. (a) Definition of the radical plane between two spheres. MP_i and MP_j are tangent to the spheres. (b) Radical Voronoi graph (radical planes in plain lines) of spheres in the vicinity of a plane. The Voronoi graph that would be obtained by tessellating spheres centers is superimposed for comparison (bisector planes with dashed lines).

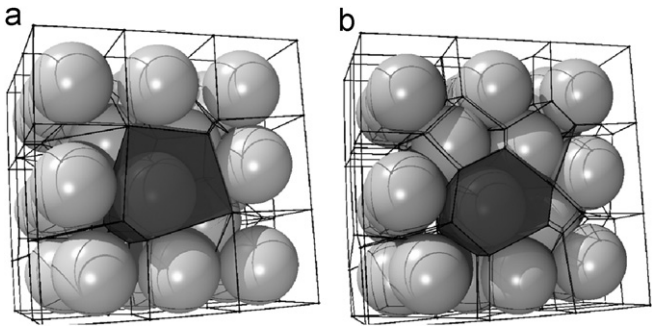

Fig. 4. View (from top) of the radical Voronoi graph of the packing (a) at initial state and (b) after die compaction. The facets of the polyhedron associated to a specific sphere are shaded for visualization.

of volume V_s is defined as

$$\rho_i = \frac{V_s}{V_i}, \tag{3}$$

V_i being the volume of the polyhedron associated to sphere i, as seen in Fig. 4.

The construction of the Voronoi graph has been implemented in YADE using the open source library Computational Geometry Algorithms Library [5], which offers a flexible and efficient set of functions to construct the Delaunay and Voronoi graphs. This library gives the best possible scaling in terms of computation time, as the algorithm complexity of constructing the graphs scales linearly with the number of points [31]. The Voronoi graph of the 32-sphere assembly is shown in Fig. 4 for low and high relative density. The graph is updated at each time-step, so that the values of local solid fraction reflect the volume change of the packing.

3.2. Elastic–plastic high-density model

In Harthong et al. [23], a DEM contact law is presented, to perform DEM simulations of high-density compaction. This work is based on finite element analyses of particular periodic lattices which give information on high-density effects on the contact forces. The finite element simulations, based on the material defined in Section 2.1, show that the increase of the contact force linked to interactions between neighboring contacts is related to plastic incompressibility. Consequently, the local solid fraction parameter ρ_i defined by Eq. (3) is introduced to take into account the incompressibility of particles, by imposing the condition that the contact force has a vertical asymptote when the local solid fraction tends to 1 (in practice, the solid fraction can be slightly higher than 1 because of elastic compressibility).

At the contact level between spheres i and j, the average local solid fraction is defined as

$$\rho_{ij} = \tfrac{1}{2}(\rho_i + \rho_j) \tag{4}$$

The contact law of Harthong et al. [23] is formulated for contacts between identical spheres, i.e., of the same radius R and the same material defined by σ_0 and m. The contact force is given by

$$F_{ij}^{pl}(t+\Delta t) = F_{ij}^{pl}(t) + S_{ij}^{pl}(h_{ij},\rho_{ij}).\Delta h_{ij}(t) \tag{5}$$

t being the current time and Δt the time increment, other notations are given in Fig. 1. The stiffness S_{ij} is expressed as the sum of two terms:

$$S_{ij}^{pl}\left(\frac{h_{ij}}{R},\rho_{ij},n\right) = S_1\left(\frac{h_{ij}}{R},n\right) + S_2(\rho_{ij},n) \tag{6}$$

where S_1 represents the indentation force for an isolated contact, corresponding to the simple compression of an isolated sphere (Eq. (7) is valid up to $h_{ij}/R = 1$):

$$\frac{S_1}{\sigma_0 R} = \alpha_1(m)\exp\left(\beta_1(m)\frac{h_{ij}}{R}\right) + \gamma_1(m)\exp\left(-\delta_1\frac{h_{ij}}{R}\right) \tag{7}$$

and S_2 corresponds to an increase of the contact force caused by plastic Von Mises incompressibility and interactions between neighboring contacts. Its form ensures that S_2 is zero or negligible when ρ_{ij} is close to its initial value ρ_{ij}^0, and it tends to infinity when ρ_{ij} tends to 1:

$$\frac{S_2}{\sigma_0 R} = \alpha_2(m)\frac{[\max(0,\rho_{ij}-\rho_{ij}^{\mathrm{ref}})]^2}{1-\rho_{ij}} \tag{8}$$

ρ_{ij}^{ref} is a reference local solid fraction. In Harthong et al. [23], ρ_{ij}^{ref} is the average local solid fraction when the contact appears. In the present work it is replaced by

$$\rho_{ij}^{\mathrm{ref}} = \max(\rho_0^{\min},\rho_{ij}^0) \tag{9}$$

where ρ_{ij}^0 is the value of ρ_{ij} in the undeformed assembly, and $\rho_0^{\min}$ is an average minimal value, under which a sphere cannot develop any resistance to compressibility. This choice implies that:

- If the average local solid fraction ρ_{ij} in the undeformed assembly is lower than $\rho_0^{\min}$, resistance to compressibility (represented by S_2) only appears when ρ_{ij} reaches $\rho_0^{\min}$.
- If the average local solid fraction ρ_{ij} in the undeformed assembly is higher than $\rho_0^{\min}$, and spheres i and j are initially in contact, resistance to compressibility appears immediately at the beginning of the loading (S_2 is zero and increases with compaction).
- If the average local solid fraction ρ_{ij} in the undeformed assembly is higher than $\rho_0^{\min}$, but spheres i and j are not initially in contact, then resistance to compressibility appears when the contact appears. But, in this case, S_2 is nonzero when the contact appears,[1] and consequently the total stiffness S_{ij}^{pl} is higher. This expresses that the spheres already developed resistance to compressibility through the preceding contacts.

In practical terms, we chose $\rho_0^{\min} \simeq 0.52$, which is the initial solid fraction[2] of the simple cubic structure which has been used to calibrate Eq. (6) [23].

Then, the parameters $\alpha_1,\beta_1,\gamma_1,\delta_1$ and α_2 are defined as

$$\begin{cases} \alpha_1(m) = 0.97 - \dfrac{0.58}{m} \\ \beta_1(m) = 1.75\left(1+\dfrac{1}{2m}\right) \\ \gamma_1(m) = \dfrac{15m}{3+m} - 4 \\ \delta_1 = 8 \\ \alpha_2(m) = 15\left(1-\dfrac{1}{2m}\right) \end{cases} \tag{10}$$

Eqs. (6)–(10) are intended to cover the whole range of m from 1 (linear stress–strain relationship) to ∞ (perfect plasticity), and a range of h/R from 0 to 1.

Using Eq. (3) as a definition for the local solid fraction, this plastic model can be implemented in a DEM code, but elasticity and friction must also be considered to include qualitative effects in the simulations, in particular in the rearrangement stages

[1] The contact force is zero when the contact appears, but S_1 is nonzero in any case, and S_2 is zero or nonzero, depending on the situation.

[2] Because of periodicity, the local solid fraction is equal to the relative density in this case.

where elastic unloading and friction are involved. We introduced a constant linear elastic stiffness k_n^{el} in the normal direction, and k_t^{el} in the tangent direction. Since the present study is limited to monotonic compressive loadings, it may be acceptable to scale the elastic stiffness to a value lower than the physical one, in order to limit computation time (increased time increment). This approach implies that the physical elastic stiffness (which is known to be nonlinear and history dependent) is too high to be represented with the time increments used in our simulations. Then, the chosen value is the maximum stiffness k_n^{el} compatible with the size of the time increment (usually chosen as a fraction of $\sqrt{M/k_n^{el}}$, where M is the mass of the smallest particle).

Using such a model results in an underestimation of the stiffness at high relative density. However, higher stiffnesses can be reached with longer simulations or by increasing the time step before reaching the critical value of relative density, which can be easily calculated from Eqs. (6)–(10), and decreasing it afterwards. The actual value of stiffness and time step used in this work actually depended on the simulations. For instance, the value of the plastic adimensional stiffness $S_{ij}^{pl}/\sigma_0 R$ predicted by the high-density model for $h/R=0.75$ and $\rho_{ij}=0.95$ (this values correspond to die compaction of the simple cubic cell as presented in Fig. 14) is approximately 51. This value corresponds to a stiffness $S_{ij}^{pl}=1.62\times10^5$ N m^{-1}. Using a safety coefficient of 0.5 for the time step in the DEM simulations, along with a volumic mass of 11,400 kg m^{-3} and monosized spheres of initial radius 0.153 mm, the time step required to get this stiffness is 5.1×10^{-7} s. The influence of the scaling of the elastic stiffness for local unloading is expected to be really negligible since local unloading only happened during the rearrangement phase in our simulations, which only concerns low relative densities and very low relative displacement ranges.

The direction of the tangential force F_{ij}^t is defined by the direction of the incremental tangential displacement. The magnitude of F_{ij}^t is increased gradually, with stiffness k_t^{el}, and is thresholded during the sliding stage to fF_{ij}^n, where f is the friction coefficient. A simple expression for k_t^{el} is adopted:

$$k_t^{el}=0.5k_n^{el} \tag{11}$$

Combining elastic and plastic stiffnesses, a classical elastic–plastic model is formulated by assigning an elastic or plastic stiffness depending on whether the contact is unloading/reloading or in the plastic regime.

To ensure convergence, the plastic stiffness must not tend to infinity. Therefore, in the case of the high-density model, S_{ij}^{pl} (defined by Eq. (6)) is limited as follows:

$$S_{ij}^{pl\prime}=\min(S_{ij}^{pl},k_n^{el}) \tag{12}$$

Fig. 5 illustrates the normal force obtained under these considerations.

3.3. Die compaction of a 32-sphere assembly

The stress response of a representative random assembly of spheres to every loading direction in the stress space is of critical importance to derive a constitutive law for continuum finite element analyses. Here our 32-sphere sample is not representative of a continuum material, and it is only intended to compare the results of the two methods in a reasonable calculation time. It should be emphasized that the high-density model only evaluates the normal contact force. Very simplified tangential or rotational behavior is implemented in the present DEM simulations. As a result, it is not expected that comparable kinematics will be obtained with both methods.

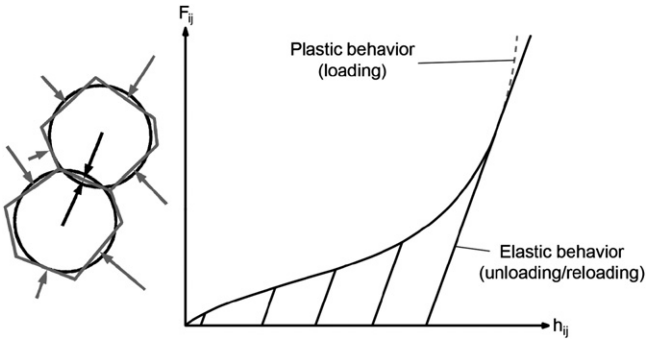

Fig. 5. Illustration of the contact normal force, for cyclic loadings. For clarity, the elastic stiffness is very much softened.

Comparison between MPFEM and DEM simulations, with the high-density model and with Storåker's model for 32-sphere assemblies, is presented in Jerier et al. [27] in the case of frictionless particles. Both isotropic and die compaction are studied in this preceding paper. The 32-sphere assembly is compressed by rigid walls using both methods. The macroscopic wall stresses, defined as the resulting forces on each wall, divided by the corresponding current area, were recorded together with the overall relative density during die and isotropic compression tests. Fig. 6 shows the wall stresses – relative density curves for the 32-sphere assembly under die compaction with a friction coefficient $f=0.1$. For this loading, all four lateral walls remain fixed and the compaction is made by the displacement of both axial walls along the Z-direction. Fig. 6 shows a good agreement between DEM and MPFEM up to a density of 0.95 with the high-density model, with a small discrepancy for the Z-Wall. The DEM with Storåkers's law gives valuable predictions only up to a relative density of about 0.9. Note in passing that the DEM simulations have been stopped at a relative density of 0.95, because this value was considered large enough to cover industrial needs. However, local validation of the high-density model has been achieved using MPFEM up to a relative density up to 0.98 (see Figs. 14 and 7 for instance) showing that the high-density model can capture the behaviour of contact forces up to this value of relative density.

This shows that the contact normal force derived from the high-density model in the DEM leads to a good concordance with the MPFEM for the stresses. The simplified tangential force implemented accounts for frictional effects in a rather satisfying way. Furthermore, Storåkers's model leads to a correct prediction up to relative densities of about 0.85 for the macroscopic wall stresses. As an additional remark, isotropic and die compaction, which have been tested here and in Jerier et al. [27], are quite representative of the loadings involved in the industrial densification processes, and it is expected that the results shown here can be considered as valid for the range of stresses with similar triaxialities. Thus it seems that the macroscopic wall stresses are closely linked with the contact normal force. However, it is expected that the contribution of the tangential contact force increases when the loadings become more deviatoric. In industrial processes, friction against the walls and geometric singularities can lead to highly deviatoric loadings, which are of particular importance as they can result in cracking problems. The present paper does not account for cracking, as it appears senseless in the absence of cohesion, but the question of whether the response from both methods is similar or not under highly deviatoric stresses remains an open question.

Fig. 7 shows the evolution of the contact force for a single contact chosen in the 32-sphere packing. Two spheres are selected in the central part of the assembly and have no contact

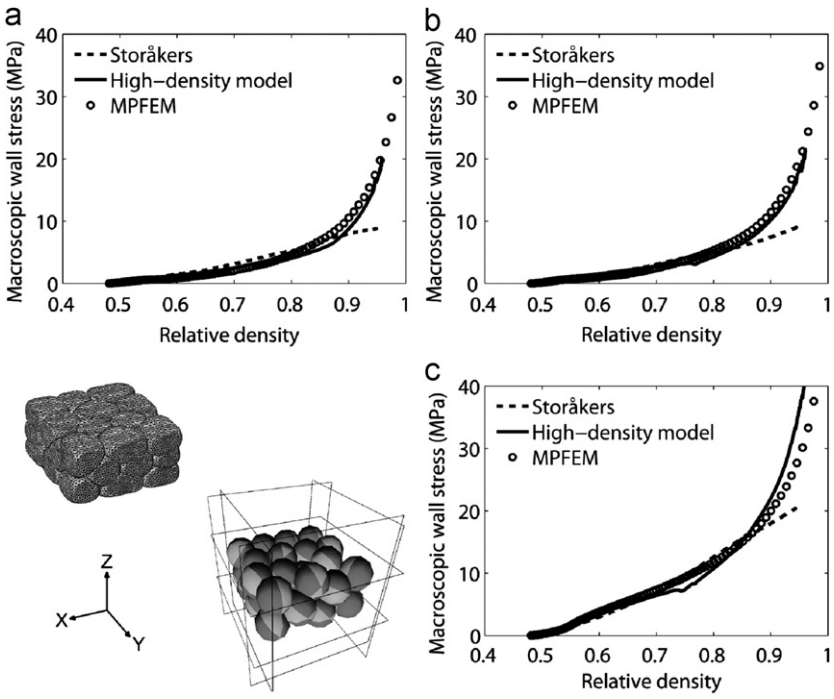

Fig. 6. Comparison between DEM and MPFEM stress–density curves for die compaction of 32 lead spheres in random packing with friction ($f=0.1$). The stresses are measured along: (a) the *X*-axis, (b) the *Y*-axis, and (c) the *Z*-axis.

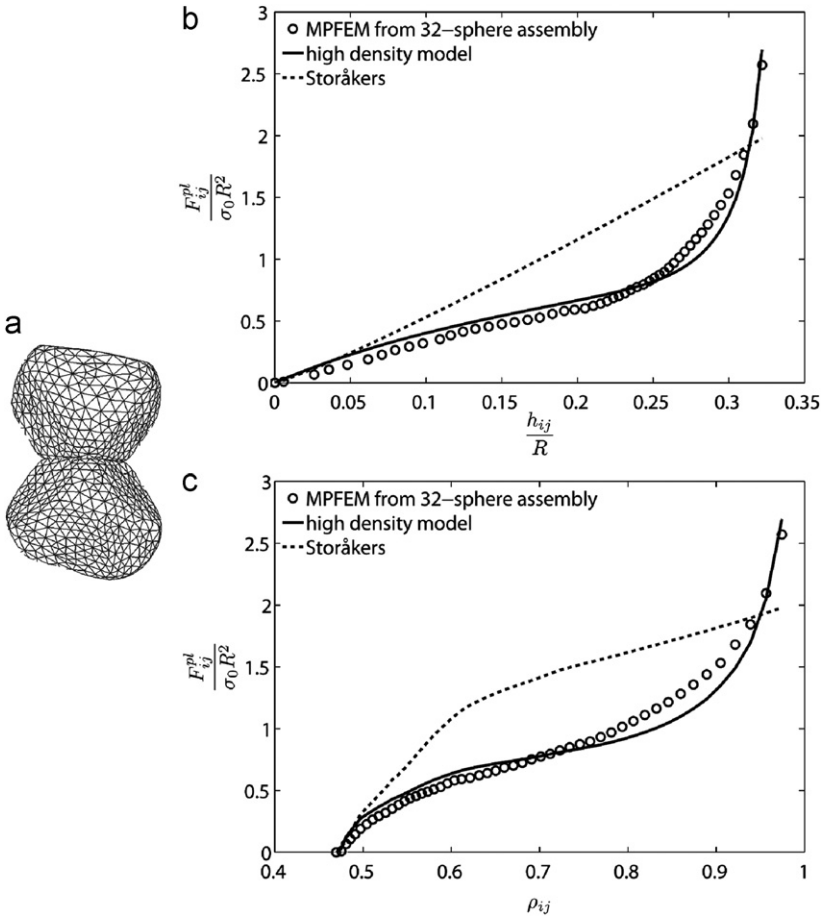

Fig. 7. Evolution of the contact force between two spheres in an assembly of 32 spheres under isotropic compaction. (a) Deformed configuration of the spheres in contact. (b) Contact force as a function of the indentation depth. (c) Contact force as a function of the average local solid fraction. Due to the small number of particles in the packing, the local solid fraction is quite homogeneous, so that the evolution of the local solid fraction ρ_{ij} is very close to the evolution of the macroscopic density D of the packing. Both quantities evolve from 0.48 to 0.98 during the MPFEM simulation.

with the compressing walls, in order to avoid potential edge effects. Furthermore, these spheres are in contact in the undeformed configuration, to avoid the difficulties linked with the tracking of new contacts appearing during compaction [23]. While the assembly is submitted to an isotropic compaction, the positions of the central node of each of the 32 spheres are saved. These data are then used to calculate a relative displacement h_{ij} and to build the Voronoi cells of the two studied spheres, to finally derive an average local solid fraction ρ_{ij} from MPFEM simulations.

This approach assimilates the center of a sphere (in the sense of the DEM) to the central node of the meshed sphere in the MPFEM; but we believe that this leads to a good approximation of the evolution of the local solid fraction. It is thus possible to obtain information on how the high-density model represents the normal contact force in several configurations, by separating the normal contact force from friction, rotations or other contributions, which may differ between MPFEM and DEM and lead to significant differences in the kinematics. Under these assumptions, the evolution of the contact force between the chosen spheres is shown in Fig. 7 as a function of h_{ij} and ρ_{ij}, from the MPFEM, the high-density model and Storåkers's model. In this case, the latter overestimates the contact force up to $\rho_{ij} \simeq 0.95$ while the high-density model shows a correct agreement with the MPFEM. As an effect of confinement, the contact force increases significantly for $\rho_{ij} > 0.8$, such that it eventually becomes higher than predicted by Storåkers's model beyond the value of 0.95. As a remark, it is noteworthy that if the force–displacement relationship predicted by Storåkers model seems linear, it is actually not. The non-linearity of the curve shown in Fig. 7b is difficult to see because it mainly concerns a range of h/R values smaller than 0.05. This can be double-checked in Fig. 10.

The theory of Storåkers and co-workers is known to give valuable predictions up to relative densities of about 0.85 when associated to the DEM [34]. This result shows that, despite this, it does not reproduce the local contact force very well in some particular cases. Although this example is just a particular case, it raises the fact that Storåkers model only gives valuable results in average. Using Storåkers model would thus result in overestimating the contact force of some contacts and underestimating the contact force of other contacts. The macroscopic average stresses can be expected to be accurate up to a relative density of at least 0.8. However, local information such as for example, distribution of relative density, should not be expected to be reliable for relative densities as low as 0.5 or 0.6. This issue is investigated in details in Section 4.

4. Discussion: normal contact force in high-density compaction

To make this point clearer, and explore further the local mechanisms which rule the normal contact force, three stages of the compaction are explored: spherical indentation, with large displacements (Section 4.1); contact interactions (Section 4.2); and high-density behavior (Section 4.3). Thus, the 32-sphere assembly is exploited, but it also seems useful to introduce some results from single-sphere simulations. Single-sphere models easily give the contact forces on one single particle while keeping a reasonable size for the output files. The models simulate two isolated spheres indenting each other (Fig. 8a) and a simple cubic elementary cell under isotropic (Fig. 8b) or die (Fig. 8c) compaction.

The finite element meshes are shown in Fig. 9. For simple compression, the mesh is refined in the contact region to obtain reliable results on contact surfaces (Fig. 9b).

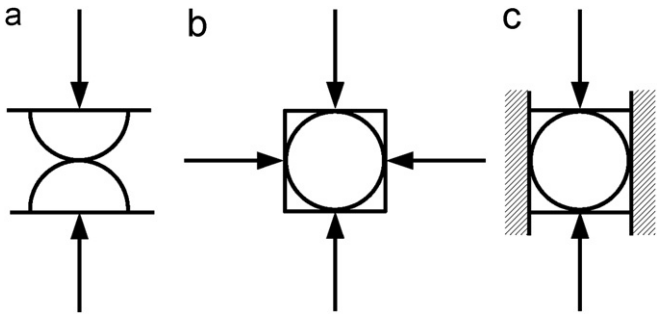

Fig. 8. Single-sphere loadings: (a) simple compression of two spheres; (b) isotropic compaction of a simple cubic periodic cell; (c) die compaction of a simple cubic periodic cell.

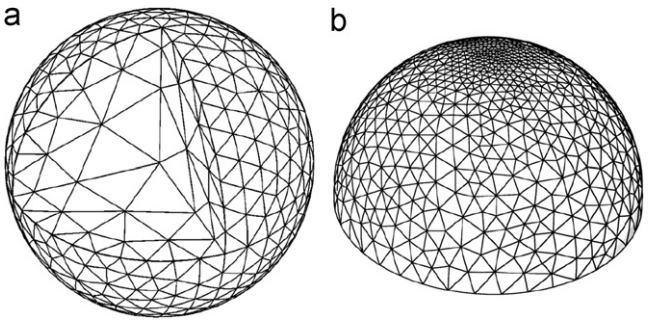

Fig. 9. Finite element meshes (a) for a single sphere, and (b) for the study of contact surfaces in simple compression.

4.1. Simple compression (spherical indentation with large displacements)

Spherical indentation is studied here through the simple compression test defined in Fig. 8a. The results of non-linear deformation can thus be separated from confinement or contact impingement. This section compares results from MPFEM and contact models from Section 3 to underline the range of h_{ij}/R where the models are valid. Moreover, we try to quantify the range of h_{ij}/R expected to be useful in the modeling of high-density compaction.

Fig. 10 shows the force–displacement curves obtained for a simple compression with MPFEM simulations, Storåkers's model and the high-density model. For the high-density model, it is considered that $\rho_{ij} = 0$ (a sphere in a cell of infinite volume), such that the stiffness reduces to S_1 defined by Eq. (7). The material parameters correspond to lead (cf. Eq. (2)). For comparison needs, two fictitious materials are also used, with the same parameters except m (equal to infinity and 1.67). The radius of the spheres is $R = 1$ mm.

Fig. 10 shows that for a fixed value of h_{ij}/R, the contact force is an increasing function of parameter m, as a consequence of Eq. (1). For small values of m ($m = 1.67$ and lower values), all three curves are similar, and for high values of m and large values of h_{ij}/R, Storåkers's model tends to greatly overestimate the response whereas the high-density model still gives a good approximation when compared with the MPFEM results. In any case, the former model is correct for small displacements (zoom in Fig. 10). These results are to be compared with those of Mesarovic and Fleck [35], which also show that Storåkers's model is limited to an order of magnitude of about 0.1 for h_{ij}/R in the case of two deformable spheres indenting each other. However, their study is limited to h_{ij}/R about 0.2.

The lack of agreement between MPFEM and Storåkers's theory for large h_{ij}/R can be further understood by comparing the contact

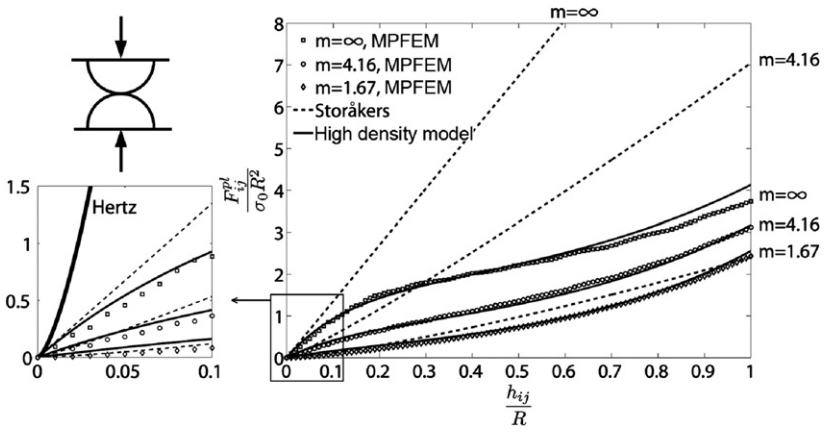

Fig. 10. Force–displacement curves given by the three models (MPFEM, Storåkers's theory and high-density model).

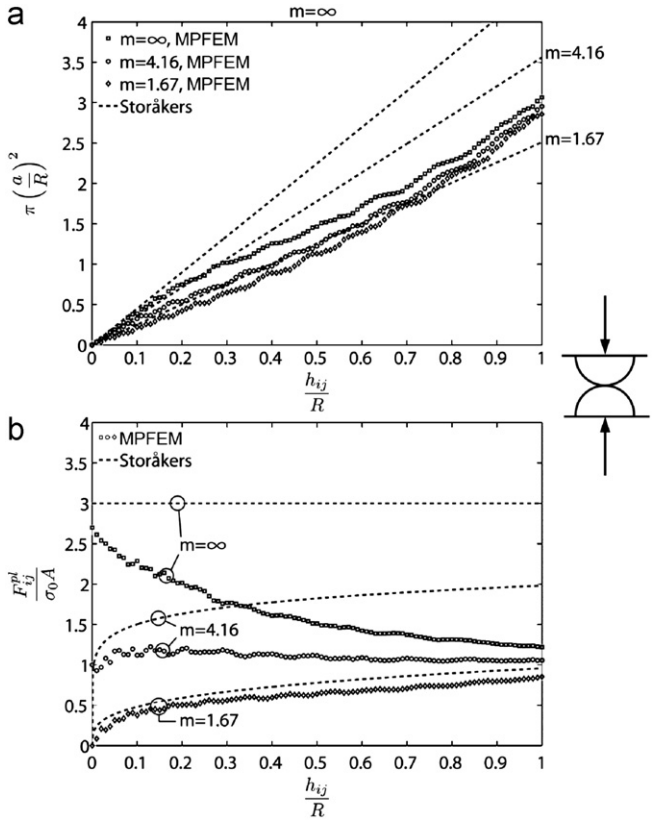

Fig. 11. Results of a simple compression test, for $m=\infty$, $m=4.16$ and $m=1.67$, according to MPFEM and Storåkers's theory. (a) Contact area and (b) average contact pressure (resulting force divided by contact area). a is the radius of the contact area, corresponding to each model, and A is the contact area.

area and pressure given by both methods, since these quantities are predicted by the latter theory. Fig. 11a shows the evolution of the contact area predicted by Storåkers's model and MPFEM simulations in the case of simple compression. The first model predicts a higher contact area than the MPFEM for high values of h_{ij}/R and m. MPFEM results show that the evolution of the contact area between two spheres is nonlinear. The small jumps on the MPFEM curves are caused by insufficient mesh refinement, because the value of the contact area is highly influenced by the size of the elements compared to the size of the contact area.

Fig. 11b shows the average pressure (normalized by σ_0) on the contact surface. In this case Storåkers's theory obviously disagrees with MPFEM predictions. In particular, his model assumes that for perfect plasticity ($m\to\infty$), the contact pressure is independent of the indentation depth h_{ij}/R and is equal to $3\sigma_0$. MPFEM results, on the contrary, show that the contact pressure decreases from about $3\sigma_0$ towards σ_0. This effect clearly relies in the change in shape of the sphere, which is not considered in Storåkers's theory.

This underlines the fact that his assumption of small displacements (such that contact surfaces remain small compared with the size of the contacting bodies, see [43]) is not valid at this scale, at least for high values of m. We do not know the amplitude of relative displacement which has to be considered for high-density compaction in the general case. However, it is possible to obtain data from the example of our 32-sphere packing with an initial relative density $D=0.48$. By tracking the nodes of the finite element mesh which initially correspond to the centers of the particles, the indentation depths were measured. Two indicators are taken: the average indentation depth h_{av}/R and the maximum indentation depth h_{max}/R. These results reveal that:

- For isotropic compaction:
  At $D=0.98$, $h_{av}/R=0.28$ and $h_{max}/R=0.59$.
  At $D=0.8$, $h_{av}/R=0.21$ and $h_{max}/R=0.42$.
- For die compaction:
  At $D=0.98$, $h_{av}/R=0.33$ and $h_{max}/R=1$.
  At $D=0.8$, $h_{av}/R=0.25$ and $h_{max}/R=0.73$.

With these values, Storåkers's model does not appear reliable for the modeling of the compaction of the 32-sphere assembly even up to $D=0.8$. On the other hand, the high-density model is formulated to fit the data up to $h_{ij}/R=1$ with Eq. (7). But before concluding about this model, it is helpful to study the influence of contact interactions on the contact force.

4.2. Contact interactions

It is not easy to obtain quantifiable data on contact interactions. One possibility lies in the comparison between force–displacement curves in simple compression and in other situations including confinement effects. The present section proposes a comparison between color maps of stresses and strains inside the grains – which indicate structural changes inside the grains – and curves obtained through numerical tests on a simple cubic structure as defined in Fig. 8.

Fig. 12 shows the contact areas (enlightened by a color map of the contact pressure) on a sphere, chosen in the assembly, at six different states along the compaction corresponding to overall relative densities (D) of 0.55, 0.6, 0.7, 0.8, 0.9 and 0.98. The deformed shapes give an illustration of the size of the contact

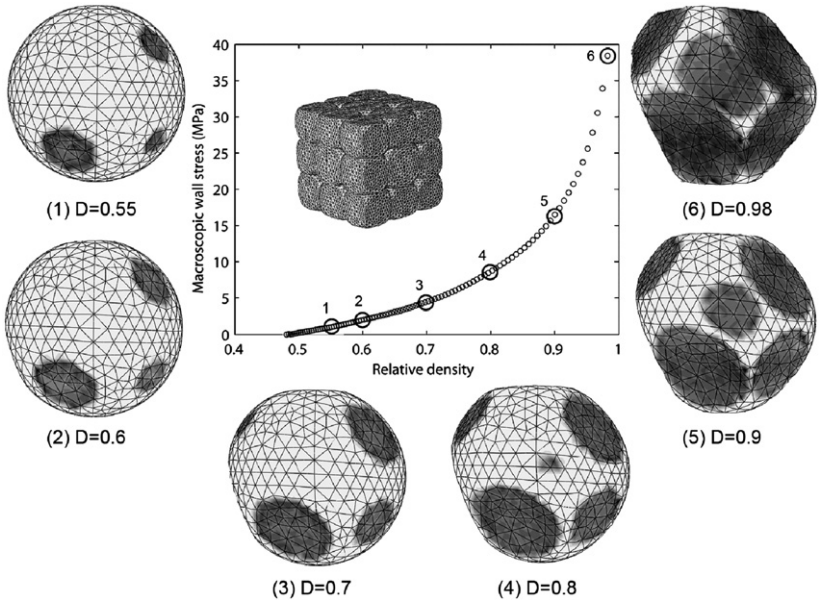

Fig. 12. Contact areas as the relative density increases.

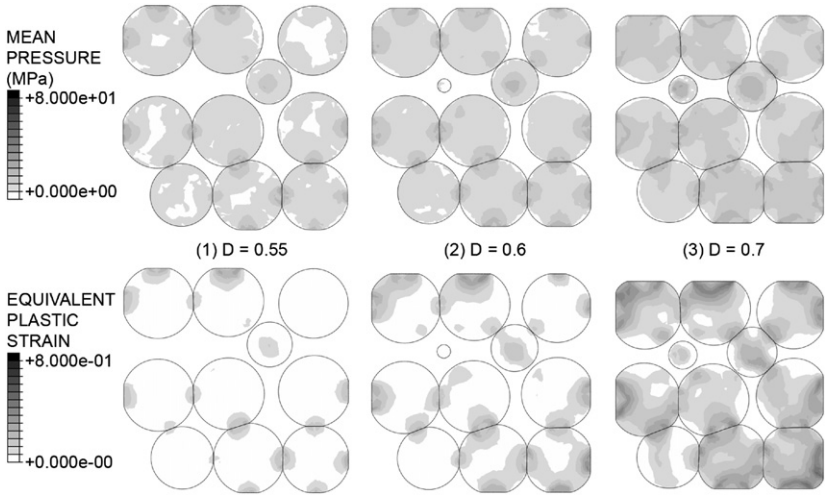

Fig. 13. Evolution of equivalent plastic strain and mean pressure in a view cut of the 32-sphere assembly, predicted by the MPFEM, in the first part of the compaction.

areas at different relative densities, and show that the contact surfaces are impinging at $D=0.9$.

Fig. 13 illustrates the evolution of the mean pressure and of the equivalent plastic strain in a view cut of the whole 32-sphere assembly. The equivalent plastic strain may be interpreted as an indicator of the increasing resistance to deformation due to strain hardening, and thus the interactions between the contacts are visible when "bridges" of plastically deformed material appear on the color map between contacts. The mean pressure is to be linked with the material's resistance to compression. Again, the bridges of mean pressure illustrate the link between resistance to compression and contact interactions.

In Fig. 13, the bridges begin to appear close to the compressing walls at $D=0.6$ (as an effect of friction), but they are visible on most spheres at $D=0.7$. In parallel, the evolution of the contact force can be studied from simulations on the simple cubic cell. Fig. 14 illustrates the influence of confinement in this very specific case, for lead ($m=4.16$). When compared with the simple compression of a single sphere, the contact forces are identical for low values of h_{ij} and becomes increasingly higher as loading proceeds (Fig. 14a). Fig. 14b suggests that this increase in force is directly related to ρ_{ij} such that $\rho_{ij}=1$ appears to be an asymptotic value (because of plastic Von Mises incompressibility, if elastic compressibility is neglected).

In Fig. 14a, the difference between isolated contacts (represented by the MPFEM simple compression curve) and interacting contacts (represented by the compaction of simple cubic cells) appears for $h_{ij}/R \simeq 0.18$ ($D=0.695$) for isotropic compaction and for $h_{ij}/R \simeq 0.50$ ($D=0.698$) for die compaction. In addition, Fig. 13 suggests that contact interactions are active at $D=0.7$. This seems to indicate that the limit between independent and interacting contacts should be 0.7 rather than 0.85 as commonly assumed.

However, in Fig. 14, the increase of the force caused by contact interactions is balanced by the overestimation given by Storåkers's model. As a result, the model fits quite well the MPFEM curve of the isotropic compaction up to $\rho_{ij} \simeq 0.9$ and $h_{ij}/R \simeq 0.33$, even though it is already critical for $h_{ij}/R=0.2$ when compared with the simple compression MPFEM curve. For die compaction, similar observations may be made, but the agreement between MPFEM and Storåkers's model is not satisfactory because the effect of

incompressibility is very late for this specific loading, and the displacement h_{ij}/R required to reach full density is nearly 1.

These results show that Storåkers's model may not be appropriate to describe the local contact behavior for large strains ($h_{ij}/R > 0.1$). However, the die compaction of the simple cubic structure is not expected to be representative of what happens in a random assembly of particles under a relatively simple loading. In a random assembly, the contact forces are distributed around the particles in a more equal manner, because of the number of contacts and their random orientations. Moreover, efficient models based on Storåkers's equations proved their efficiency up to a relative density of 0.85. It may just be noticed that this limit of 0.85 is due to the overestimation of the contact forces given by these equations for large displacements. Storåkers's model thus leads to valuable predictions for the average stresses at the macroscopic scale, but not for the local contact forces, as Fig. 7 shows. As a result, it should be used cautiously when looking at local heterogeneities, such as density distribution. However, the high-density model reproduces the contact forces in such particular cases, by relating the increase of the force to the local solid fraction.

In addition, there is a smooth transition between the assembly with independent contacts (loose powder) and dense material (compacted state), during which strain-hardening caused by contact interactions and resistance to compressibility gradually increase. We believe that this justifies the formulation of the high-density model with a gradually increasing term, modeled here as the second term S_2 (Eq. (8)).

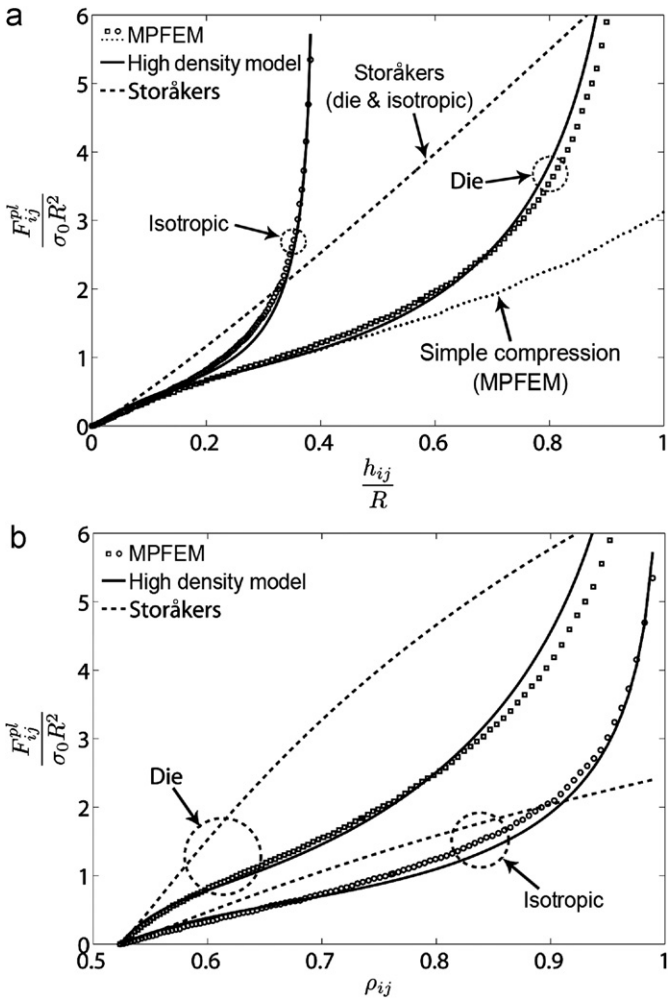

Fig. 14. Normalized contact force for $m=4.16$ as a function of the indentation depth (a) and of the relative density (b), for isotropic and die compaction of a simple cubic structure (Fig. 8b,c).

4.3. High density behavior

From the preceding results, high-density phenomena result in an asymptotic behavior where $\rho_{ij}=1$ is a limit for the indentation, the contact force becoming infinite. In Eq. (8), the force caused by the increase of the local solid fraction only depends, as a result of Eq. (4), on the local solid fraction of the contacting spheres. Except when huge differences exist in the local solid fraction of neighboring spheres, the incompressibility force is distributed in an approximately equal manner to all the contacts around the sphere. This assumes the homogeneity of this contribution; and MPFEM can give some indications on this point.

Fig. 15 is similar to Fig. 13, but for the next part of the compaction, up to $D=0.98$. These pictures show that the mean pressure tends to become quite homogeneous, except in the neighborhood of the remaining pores and in the corners, where the material is trapped between the compressing walls. In the corners, the mean pressure is really high. This is the result of an edge effect, which is quite significant because of our simplified sample with only 32 particles and no periodic boundary conditions. The homogeneity of the pressure encourages us to consider that for most spheres the resistance to compressibility can be distributed in an approximately equal manner to all the

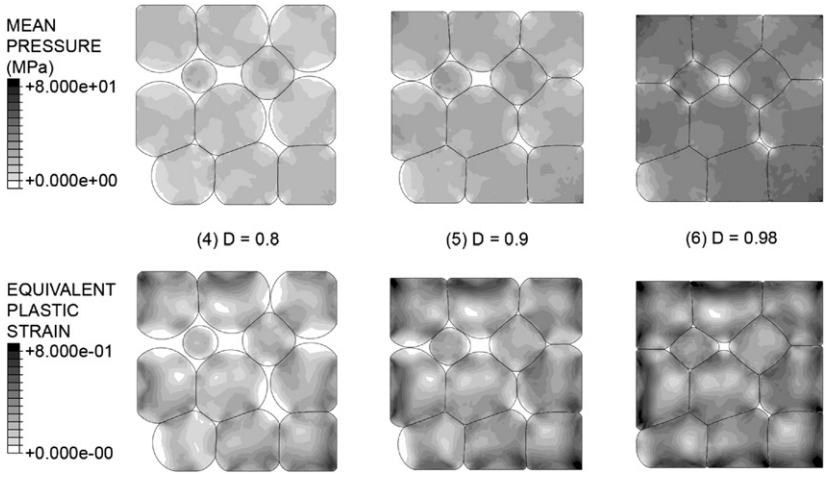

Fig. 15. Evolution of equivalent plastic strain and mean pressure in a view cut of the 32-sphere assembly, predicted by the MPFEM, in the last part of the compaction.

contacts around a sphere. Exceptions exist, as can be seen on the left-hand bottom corner, where one of the spheres' halves is much more compressed than the other. In this situation, with our present discrete element model, such a sphere would be moved a bit closer to the corner, because of the formulation of Eq. (8).

On the contrary, equivalent plastic strain is concentrated near the walls, as a well-known effect of friction. Inside the grains, the material is more deformed in the vicinity of the contacts, such that the distribution of strain is not homogeneous at all. Such complex phenomena are not considered in the high-density model, and their effects on the contact forces are included in a very coarse way in the indentation term (7) as a result of a fitting procedure on finite element results [23].

5. Concluding remarks

The description of the normal contact force for DEM modeling of high density compaction is tractable if a local solid fraction providing a correct description of contact interactions and plastic incompressibility of the constitutive material of the grains is used. The high-density model thus seems to predict the normal contact force at the contact scale with a reasonable accuracy. Furthermore, results show that a correct description of the contact forces leads to a valuable prediction of macroscopic stresses. As a result, it was also possible to obtain valuable predictions of the macroscopic wall stresses on a 32-sphere random assembly under isotropic and die compaction up to a relative density of 0.95. The present model requires only physical constants, as input parameters, linked to the constitutive material of the grains.

By completing the present contact model with cohesion and choosing an appropriate yield criterion, it would be useful to derive yield surfaces as suggested by Martin [32]. However, the complete modeling of high-density compaction with the DEM requires further investigation, as the kinematics of the particles may not be properly described by the present model. The contribution of "new" contacts appearing during compaction, discussed in Harthong et al. [23] (and already in [15]) is expected to be negligible in most cases, but the kinematics are closely linked to the modeling of friction and resistance to rotations. Iwashita and Oda [26], Plassiard et al. [37] modified the usual DEM to introduce resistance to rotation at the contact level. Martin et al. [34] consider that rotations can be simply neglected. Here we suspect that since our sample has a low initial relative density ($D_0=0.48$, to be compared with 0.64 in [34]), the rotations could have a non-negligible influence on rearrangement between 0.48 and 0.64. Such points have to be considered to obtain comparable results with both methods, in order to describe properly the density or stress distribution.

References

[1] ABAQUS, 2009. ABAQUS Version 6-8-3, User documentation. Dassault systèmes Simulia.
[2] Akisanya AR, Cocks ACF, Fleck NA. The yield behaviour of metal powders. Int J Mech Sci 1997;39:1315–24.
[3] Arzt E. The influence of an increasing particle coordination on the densification of spherical powders. Acta Metall 1982;30:1883–90.
[4] Bhushan B. Modern tribology handbook, vol. 1. LLC: CRC Press; 2001.
[5] Boissonnat J-D, Devillers O, Pion S, Teillaud M, Yvinec M. Triangulations in CGAL. Comput Geometry: Theory Appl 2002;22:5–19.
[6] Chen Y, Imbault D, Dorémus P. Numerical simulation of cold compaction of 3d granular packings. Mater Sci Forum 2006;534–536:301–4.
[7] Chen Y, Imbault D, Dorémus P. Experiment and simulation using meshed discrete particles: comparison for compaction of 3d irregular randomly packed particles. In: Proceedings of the Euro PM2008, vol. 3. European Powder Metallurgy Association; 2008. p. 139–44.
[8] Cocks ACF. Constitutive modelling of powder compaction and sintering. Prog Mater Sci 2001;46:201–29.
[9] Cocks ACF, Sinka IC. Constitutive modelling of powder compaction—i. Theoretical concepts. Mech Mater 2007;39:392–403.
[10] Cundall PA, Strack ODL. A discrete numerical model for granular assemblies. Geotechnique 1979;29:47–65.
[11] Drucker DC, Gibson RE, Henkel DJ. Soil mechanics and work-hardening theories of plasticity. Trans ASCE 1957;122:338–46.
[12] Drucker DC, Prager W. Soil mechanics and plastic analysis or limit design. Q J Mech Appl Math 1952;10:157–75.
[13] Edelsbrunner H, Shah NR. Incremental topological flipping works for regular triangulations. Algorithmica 1996;15:223–41.
[14] Federzoni L, Riedel H, Coube O, Oldenburg M, Häggblad HA, Gethin DT, et al. State of the art review—comparison of computer models representing powder compaction process. Powder Metal 1999;42:301–11.
[15] Fischmeister HF, Artz E. Densification of powders by particle deformation. Powder Technol 1983;26:82–90.
[16] Fleck NA. On the cold compaction of powders. J Mech Phys Solids 1995;43:1409–31.
[17] Fleck NA, Kuhn LT, McMeeking RM. Yielding of metal powder bonded by isolated contacts. J Mech Phys Solids 1992;40:1139–62.
[18] Frenning G. An efficient finite/discrete element procedure for simulating compression of 3d particle assemblies. Comput Methods Appl Mech Eng 2008;197:4266–72.
[19] Frenning G. Compression mechanics of granule beds: a combined finite/discrete element study. Chem Eng Sci 2010;65:2464–71.
[20] Gethin DT, Lewis RW, Ransing RS. A discrete deformable element approach for the compaction of powder systems. Model Simul Mater Sci Eng 2003;11:101–14.
[21] Gethin DT, Ransing RS, Lewis RW, Dutko M, Crook AJL. Numerical comparison of a deformable discrete element model and an equivalent continuum analysis for the compaction of ductile porous material. Comput Struct 2001;79:1287–94.
[22] Harthong B, Dorémus P, Imbault D. The study of relations between loading history and yield surfaces in powder materials using discrete finite element simulations. J Mech Phys Solids 2012;60:784–801.
[23] Harthong B, Jérier J-F, Dorémus P, Imbault D, Donzé F-V. Modeling of high-density compaction of granular materials 3 by the discrete element method. Int J Solids Struct 2009;46:3357–64.
[24] Heyliger PR, McMeeking RM. Cold plastic compaction of powders by a network model. J Mech Phys Solids 2001;49:2031–54.
[25] Hill R, Storåkers B, Zdunek A. A theoretical study of the Brinell hardness test. Proc R Soc London Ser A 1989;423:301–30.
[26] Iwashita K, Oda M. Micro-deformation mechanism of shear banding process based on modified distinct element method. Powder Technol 2000;109:192–205.
[27] Jerier J-F, Harthong B, Richefeu V, Chareyre B, Imbault D, Donze F-V, et al. Study of cold powder compaction by using the discrete element method. Powder Technol 2011;208(2):537–41.
[28] Johnson KL. The correlation of indentation experiments. J Mech Phys Solids 1970;18:115–26.
[29] Kozicki J, Donzé F-V. A new open-source software developed for numerical simulations using discrete modelling methods. Comput Methods Appl Mech Eng 2008;197:4429–43.
[30] Kozicki J, Donzé F-V. Yade-open DEM: an open-source software using a discrete element method to simulate granular material. Eng Comput 2009;26–27:786–805.
[31] Liu Y, Snoeyink J. A comparison of five implementations of 3d delaunay tessellation. In: Pach J, Goodman JE, Welzl E, editors. Combinatorial and computational geometry. MSRI Publications; 2005. p. 439–58.
[32] Martin CL. Elasticity, fracture and yielding of cold compacted metal powders. J Mech Phys Solids 2004;52:1691–717.
[33] Martin CL, Bouvard D. Study of the cold compaction of composite powders by the discrete element method. Acta Mater 2003;51:373–86.
[34] Martin CL, Bouvard D, Shima S. Study of particle rearrangement during powder compaction by the discrete element method. J Mech Phys Solids 2003;51:667–93.
[35] Mesarovic SD, Fleck NA. Frictionless indentation of dissimilar elastic–plastic spheres. Int J Solids Struct 2000;37:7071–91.
[36] Pizette P, Martin CL, Delette G, Sornay P, Sans F. Compaction of aggregated ceramic powders: from contact laws to fracture and yield surfaces. Powder Technol 2010;198:240–50.
[37] Plassiard JP, Belheine N, Donzé F. A spherical discrete element model: calibration procedure and incremental response. Granular Matter 2009;11–5:293–306.
[38] Procopio AT, Zavaliangos A. Simulation of multi-axial compaction of granular media from loose to high relative densities. J Mech Phys Solids 2005;53:1523–51.
[39] Schmidt I, Kraft T, Riedel H. Numerical homogenisation of elasto-plastic granule assemblies using discretised particles. In: Proceedings of the Euro PM2008. European Powder Metallurgy Association; 2008. p. 169–73.
[40] Sinka IC, Cocks ACF. Constitutive modelling of powder compaction—ii. Evaluation of material data. Mech Mater 2007;39:404–16.
[41] Skrinjar O, Larsson P-L. On discrete element modelling of compaction of powders with size ratio. Comput Mater Sci 2004;31:131–46.
[42] Sridhar I, Fleck NA. The yield behaviour of cold compacted composite powders. Acta Mater 2000;48:3341–52.

[43] Storåkers B, Biwa S, Larsson P-L. Similarity analysis of inelastic contact. Int J Solids Struct 1997;34:3061–83.
[44] Storåkers B, Fleck NA, McMeeking RM. The viscoplastic compaction of composite powders. J Mech Phys Solids 1999;47:785–815.
[45] Šmilauer V, Catalano E, Chareyre B, Dorofenko S, Duriez J, Gladky A, et al. Yade documentation, 1st ed. The Yade Project; 2010 〈http://yade-dem.org/doc/〉.
[46] Vu-Quoc L, Zhang X. An accurate and efficient tangential force–displacement model for elastic frictional contact in particle-flow simulations. Mech Mater 1999;31:235–69.
[47] Vu-Quoc L, Zhang X, Lesburg L. Normal and tangential force–displacement relations for frictional elasto-plastic contact of spheres. Int J Solids Struct 2001;38:6455–89.
[48] Xin XJ, Jayaraman P, Daehn GS, Wagoner RH. Investigation of yield surface of monolithic and composite powders by explicit finite element simulation. Int J Mech Sci 2003;45(4):707–23.